

# Supplemental Material: Quantum-Enhanced Metrology for Molecular Symmetry Violation using Decoherence-Free Subspaces

Chi Zhang,<sup>1,\*</sup> Phelan Yu,<sup>1</sup> Arian Jadbabaie,<sup>1</sup> and Nicholas R. Hutzler<sup>1</sup>

<sup>1</sup>*California Institute of Technology, Division of Physics,  
Mathematics, and Astronomy. Pasadena, CA 91125*

The structure of the Supplemental Material is as follows:

1. In Section I, we discuss the details of the eEDM coupling in a single molecule. When the molecule is prepared in a superposition of the opposite parity doublet states it has an electric dipole moment oscillating at the splitting frequency, and an associated oscillating effective electric field. When the electron spin is polarized along a transverse direction, the interaction of the eEDM with the effective electric field will result in a spin precession which oscillates back and forth because the direction of  $\mathcal{E}_{\text{eff}}$  oscillates back and forth. It time-averages to zero. If a transverse static magnetic field is added and its magnitude tuned to match the parity splitting, the spin will stay in phase with the oscillation of  $\mathcal{E}_{\text{eff}}$  and there will be a net precession due to the eEDM. This requires an extremely stable magnetic field which is probably not feasible unless the doublet splitting is very small. Instead, an rf magnetic field can be applied along the quantization axis whose frequency matches the oscillation frequency of  $\mathcal{E}_{\text{eff}}$ . If the amplitude is strong enough, the spin follow the rf field adiabatically and there will be a net precession in the rotating frame. This method suffers from noise on the amplitude of the rf magnetic field which will wash out the eEDM signal unless the noise can be made extremely small.
2. In Section II, we show that the method using an rf magnetic field can be extended to a two-molecule system, in which the unwanted shifts from the magnetic field cancel out but the eEDM spin precession adds up linearly to molecule number (Heisenberg scaling). We also present a detailed example of an experimental sequence and show what the observables are in the lab frame.
3. In Section III, we discuss possible experimental imperfections and show that their impacts can be mitigated.
4. In Section IV, we present an example of entangling two molecules using an existing entanglement protocol.
5. In Section V, we briefly discuss the Heisenberg scaling of the eEDM sensitivity in larger entangled systems, as well as the possible ways to prepare a large entangled system.
6. In Section VI, we illustrate the optimal measurement scheme for systems with finite entangling gate errors.
7. In Section VII, we summarize the requirements for choice of molecule species for our scheme, and list some suitable molecule species.

## I. DETAILS OF THE EEDM COUPLING

In this section we present a more general and detailed description about the eEDM coupling in one molecule. Fig. S1 shows the total angular momentum excluding spins labeled as  $N$ , and its projection on the molecule axis  $K = N \cdot \hat{n}$ , which can receive contributions from orbital angular momentum and rotation about the molecule axis. For molecules with nonzero  $K$ , the good parity states are superpositions of equal and opposite  $K$  states, i.e.,  $|N, K, \pm\rangle = \frac{1}{\sqrt{2}} (|N, K\rangle \pm (-1)^{N-K} |N, -K\rangle)$ . The degeneracy between opposite parity states (i.e., a parity doublet) is lifted by high-order interactions such as the interaction with the end-to-end rotation of the molecule. For molecules with  $K = 0$ , the good parity states are rotational states  $|N\rangle$  and are split by the rotational energy. Next,  $S$  is aligned, or partially aligned, to  $N$  by spin-orbit or spin-rotation interactions with the sub-components of  $N$ . The total angular momentum formed by  $S$  and  $N$  is labeled as  $J$ . Molecule eigenstates have well-defined  $J$  and are superpositions of states of the same parity.  $S$  precess about  $J$  and the averaged  $S$  projection on  $\hat{n}$  is  $\Sigma_0$  [1]. Molecule eigenstates are superpositions of  $\pm\Sigma_0$ . In addition, nuclear spins ( $I$ ) may interact with  $J$  to form  $F$ . Here we consider the extreme  $M$  (magnetic quantum number) states with  $M = \pm F$ , where the nuclear spins are separable.

---

\* chizhang@caltech.edu

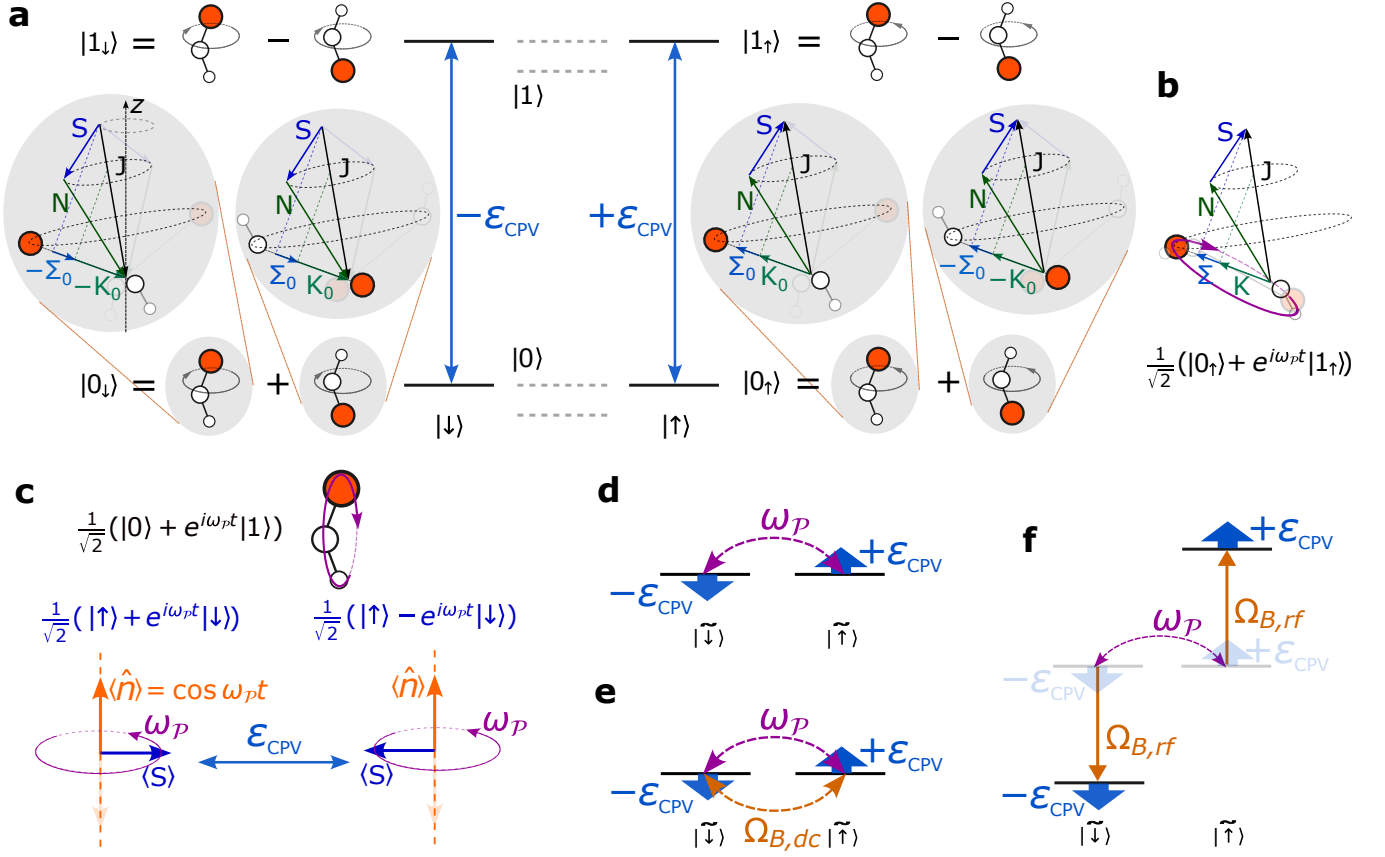


FIG. S1. (a) A more general and detailed coupling diagram of angular momenta in a molecule, similar to Fig. 1 in the main text. The arrows represent angular momenta or their projections (see text for details), the dashed circles stand for precession, i.e., the angular momentum or molecule axis is in a superposition around another axis or angular momentum and has zero expectation value perpendicular to that axis. (b) In a superposition of two opposite parity states, the molecule axis is rotating (purple arrow) while all the angular momenta are stationary. Note that the rotational axis is in a superposition (precession) about the total angular momentum  $J$  and  $J$  precess about the lab  $z$  axis, as a result, the dipole moment vanishes in the  $x, y$  plane and is oscillating along  $z$  direction. (c) In a superposition of the opposite parity states, the eEDM spin precession only happens between the spin states that rotate in phase with the molecule axis. (d) In the rotating frame, the molecule rotation couples  $|\tilde{\uparrow}\rangle$  and  $|\tilde{\downarrow}\rangle$  and suppresses eEDM spin precession. (e) The non-adiabatic method. A dc magnetic field can be used to cancel the coupling of the rotation. (f) The adiabatic method. An rf magnetic field can be used to split  $|\tilde{\uparrow}\rangle$  and  $|\tilde{\downarrow}\rangle$  and thus suppress the coupling of the rotation. The problems of (e) and (f) are explained in the text.

As in the main text, we label the positive and negative parity states as  $|0\rangle$  and  $|1\rangle$ , and the superposition  $|\uparrow\rangle = \frac{1}{\sqrt{2}}(|0\rangle + |1\rangle) = |N, K\rangle$  and  $|\downarrow\rangle = \frac{1}{\sqrt{2}}(|0\rangle - |1\rangle) = |N, -K\rangle$ . We label the spin states in the lab frame as  $|\uparrow\rangle$  and  $|\downarrow\rangle$ . The eEDM oppositely shifts the energies of the spins aligned and anti-aligned with the dipole. In the  $\{|\uparrow\rangle, |\downarrow\rangle\} \otimes \{|\uparrow\rangle, |\downarrow\rangle\}$  basis (the quantization axis is along  $z$ ), the molecular Hamiltonian including the eEDM coupling is:

$$H_{\text{pol}} = \begin{pmatrix} \epsilon_{\text{CPV}} & 0 & -\omega_p/2 & 0 \\ 0 & -\epsilon_{\text{CPV}} & 0 & -\omega_p/2 \\ -\omega_p/2 & 0 & -\epsilon_{\text{CPV}} & 0 \\ 0 & -\omega_p/2 & 0 & \epsilon_{\text{CPV}} \end{pmatrix}, \quad (1)$$

$\omega_p$  is from the higher order coupling between  $|\uparrow\rangle \leftrightarrow |\downarrow\rangle$ . The eEDM interaction causes opposite spin precession in the subspaces of  $\{|\uparrow\uparrow\rangle, |\uparrow\downarrow\rangle\}$  and  $\{|\downarrow\uparrow\rangle, |\downarrow\downarrow\rangle\}$ . However, a molecule initially prepared in  $\uparrow$  oscillates between  $\uparrow \leftrightarrow \downarrow$  at the frequency of the parity doubling  $\omega_p$ . As a result, the eEDM spin precession oscillates and averages to zero.

$H_{\text{pol}}$  can be transformed to the molecule eigenbasis ( $\{|0\rangle, |1\rangle\} \otimes \{|\uparrow\rangle, |\downarrow\rangle\}$ ) as

$$H_{\text{mol}} = \begin{pmatrix} 0 & 0 & \varepsilon_{\text{CPV}} & 0 \\ 0 & 0 & 0 & -\varepsilon_{\text{CPV}} \\ \varepsilon_{\text{CPV}} & 0 & \omega_{\mathcal{P}} & 0 \\ 0 & -\varepsilon_{\text{CPV}} & 0 & \omega_{\mathcal{P}} \end{pmatrix}. \quad (2)$$

This is the coupling shown in Fig. S1, where the eEDM only has a vanishing second order effect. In the frame rotating at  $\omega_{\mathcal{P}}$  frequency about the  $x$ -axis, the Hamiltonian is transformed by  $|0\rangle \langle 0| + e^{i\omega_{\mathcal{P}}t} |1\rangle \langle 1|$  and  $|+\rangle \langle +| + e^{i\omega_{\mathcal{P}}t} |-\rangle \langle -|$ , with  $|\pm\rangle = \frac{1}{\sqrt{2}}(|\uparrow\rangle \pm |\downarrow\rangle)$ . After neglecting the small and fast-oscillating terms proportional to  $\varepsilon_{\text{CPV}}e^{\pm i\omega_{\mathcal{P}}t}$ , the Hamiltonian is:

$$\tilde{H}_{\text{mol}} = \frac{1}{2} \begin{pmatrix} 0 & \omega_{\mathcal{P}} & \varepsilon_{\text{CPV}} & \varepsilon_{\text{CPV}} \\ \omega_{\mathcal{P}} & 0 & -\varepsilon_{\text{CPV}} & -\varepsilon_{\text{CPV}} \\ \varepsilon_{\text{CPV}} & -\varepsilon_{\text{CPV}} & 0 & \omega_{\mathcal{P}} \\ \varepsilon_{\text{CPV}} & -\varepsilon_{\text{CPV}} & \omega_{\mathcal{P}} & 0 \end{pmatrix}. \quad (3)$$

We define the rotating frame basis  $|\widetilde{\uparrow}\rangle = \frac{1}{2}(|0\rangle + e^{-i\omega_{\mathcal{P}}t}|1\rangle)$ ,  $|\widetilde{\downarrow}\rangle = \frac{1}{2}(|0\rangle - e^{-i\omega_{\mathcal{P}}t}|1\rangle)$ ,  $|\widetilde{+}\rangle = \frac{1}{2}(|+\rangle + e^{-i\omega_{\mathcal{P}}t}|-\rangle)$  and  $|\widetilde{-}\rangle = \frac{1}{2}(|+\rangle - e^{-i\omega_{\mathcal{P}}t}|-\rangle)$ . Note that this basis consists of states which are oscillating in the lab frame.  $|\widetilde{\uparrow}\rangle$  and  $|\widetilde{\downarrow}\rangle$  are eigenstates of  $\tilde{H}_{\text{mol}}$  while  $|\widetilde{+}\rangle$  and  $|\widetilde{-}\rangle$  are not. In the rotating frame basis  $\{|\widetilde{\uparrow}\rangle, |\widetilde{\downarrow}\rangle\} \otimes \{|\widetilde{+}\rangle, |\widetilde{-}\rangle\}$ , the Hamiltonian is simply

$$\tilde{H}'_{\text{pol}} = \frac{1}{2} \begin{pmatrix} \varepsilon_{\text{CPV}} & \omega_{\mathcal{P}} & 0 & -\varepsilon_{\text{CPV}} \\ \omega_{\mathcal{P}} & -\varepsilon_{\text{CPV}} & \varepsilon_{\text{CPV}} & 0 \\ 0 & \varepsilon_{\text{CPV}} & -\varepsilon_{\text{CPV}} & \omega_{\mathcal{P}} \\ -\varepsilon_{\text{CPV}} & 0 & \omega_{\mathcal{P}} & \varepsilon_{\text{CPV}} \end{pmatrix}. \quad (4)$$

In this two-by-two block matrix (in the basis of  $\{|\widetilde{\uparrow}\rangle, |\widetilde{\downarrow}\rangle\}$ ), the diagonal parts are the eEDM shifts on the spin states ( $\pm\varepsilon_{\text{CPV}}\sigma_z$ ) and the coupling between the spin states by the rotation ( $\omega_{\mathcal{P}}\sigma_x$ ). So far we have simplified the molecule orientation as a two-level systems for which there are some coupling terms between  $|\widetilde{\uparrow}\rangle$  and  $|\widetilde{\downarrow}\rangle$  subspaces. For two interacting spin-1/2 degrees of freedom (if molecule orientation was spin-1/2), these couplings indicate transverse interactions ( $XY$  interaction). However, because the real molecule orientation is not a two-level system, and it does not have a transverse dipole moment in superpositions of  $|\widetilde{\uparrow}\rangle$  and  $|\widetilde{\downarrow}\rangle$ , these couplings are not physical and need to be removed. As a result, the Hamiltonian in the basis of  $\{|\widetilde{\uparrow}\rangle, |\widetilde{\downarrow}\rangle\} \otimes \{|\widetilde{+}\rangle, |\widetilde{-}\rangle\}$  is

$$\tilde{H}_{\text{pol}} = \frac{1}{2} \begin{pmatrix} \varepsilon_{\text{CPV}} & \omega_{\mathcal{P}} & 0 & 0 \\ \omega_{\mathcal{P}} & -\varepsilon_{\text{CPV}} & 0 & 0 \\ 0 & 0 & -\varepsilon_{\text{CPV}} & \omega_{\mathcal{P}} \\ 0 & 0 & \omega_{\mathcal{P}} & \varepsilon_{\text{CPV}} \end{pmatrix}. \quad (5)$$

Now we have two decoupled subspaces, which correspond to  $|\widetilde{\uparrow}\rangle$  and  $|\widetilde{\downarrow}\rangle$ , where the spin can precess oppositely. However, the spin precession is still suppressed by the coupling caused by the rotation of the frame. As shown in Fig. S1, in a magnetic field, we find two types of schemes: a non-adiabatic one and an adiabatic one, of spin-precession between the rotating spin states. Here we explain the schemes, and discuss why they won't work for the case of a single molecule.

The non-adiabatic method is to apply a static magnetic field along the  $x$  direction that cancels the coupling of  $\omega_{\mathcal{P}}$  exactly, as shown in Fig. S1(e). More specifically, the Hamiltonian of the magnetic field is  $\tilde{H}_{B,dc} = I_2 \otimes \frac{\Omega_B}{2} \sigma_x$ , where  $I_2$  is the two-dimensional identity matrix for the molecule alignment. The total Hamiltonian is therefore

$$\tilde{H}_{\text{pol},dcB} = \frac{1}{2} \begin{pmatrix} \varepsilon_{\text{CPV}} & \omega_{\mathcal{P}} + \Omega_B & 0 & 0 \\ \omega_{\mathcal{P}} + \Omega_B & -\varepsilon_{\text{CPV}} & 0 & 0 \\ 0 & 0 & -\varepsilon_{\text{CPV}} & \omega_{\mathcal{P}} + \Omega_B \\ 0 & 0 & \omega_{\mathcal{P}} + \Omega_B & \varepsilon_{\text{CPV}} \end{pmatrix}. \quad (6)$$

This requires fine tuning and stabilization of the magnetic field strength  $\Omega_B$  to  $\omega_{\mathcal{P}}$  ( $\gtrsim 100$  kHz) within a fluctuation less than the decoherence rate (typically  $\lesssim$  Hz). This is challenging, although magnetic field stabilization to ppm level has been achieved [2] and this scheme may work for molecules with very small parity doubling [3].

The adiabatic method is to apply an oscillating or rotating magnetic field in phase with the oscillating dipole. The spin states follow the magnetic field adiabatically and rotate in phase with the molecule axis. Note that this only requires tuning the magnetic field frequency to the parity doubling frequency, which is achievable. Equivalently, in the rotating frame, as Fig. S1(f) shows, the Hamiltonian is  $\tilde{H}_{B,rf} = I_2 \otimes \frac{\Omega_B}{2} \tilde{\sigma}_z$ , and the total Hamiltonian is

$$\tilde{H}_{\text{pol,rfB}} = \frac{1}{2} \begin{pmatrix} \Omega_B + \varepsilon_{\text{CPV}} & \omega_{\mathcal{P}} & 0 & 0 \\ \omega_{\mathcal{P}} & -\Omega_B - \varepsilon_{\text{CPV}} & 0 & 0 \\ 0 & 0 & \Omega_B - \varepsilon_{\text{CPV}} & \omega_{\mathcal{P}} \\ 0 & 0 & \omega_{\mathcal{P}} & -\Omega_B + \varepsilon_{\text{CPV}} \end{pmatrix}. \quad (7)$$

For  $\Omega_B \gtrsim \omega_{\mathcal{P}}$ , a total spin precession caused by the magnetic field and the eEDM may be observed. This can also be understood equivalently as that the dressed eigenstates  $|\pm\rangle$  are superpositions with non-equal populations in  $|\uparrow\rangle$  and  $|\downarrow\rangle$ ,  $|+\rangle = \sin\theta|\uparrow\rangle + \cos\theta|\downarrow\rangle$  and  $|-\rangle = \cos\theta|\uparrow\rangle - \sin\theta|\downarrow\rangle$ , with the mixing angle  $\theta$  given by  $\tan\theta = \Omega_B/\omega_{\mathcal{P}}$ . Here  $\Omega_B$  does not need to match  $\omega_{\mathcal{P}}$ . The eEDM interaction, which splits  $|\uparrow\rangle$  and  $|\downarrow\rangle$ , causes spin precession in the dressed eigenstates  $|\pm\rangle$  since they have non-equal  $|\uparrow\rangle$  and  $|\downarrow\rangle$  components. The problem with this scheme is that the magnetic field contributes to the same spin precession as the eEDM interaction. As a consequence, magnetic field fluctuations need to be reduced to below the eEDM shift, otherwise the eEDM spin precession phase will be washed out in the magnetic field noise. Note that this is conceptually similar to the approach proposed in [4], where this problem is avoided by using magnetically-insensitive  $M = 0$  states.

However, the adiabatic method can be extended to two entangled molecules. For two non-interacting molecules, the total Hamiltonian is  $H = H_1 \otimes I + I \otimes H_2$ , where  $H_i$  ( $i = 1, 2$ ) is the single molecule Hamiltonian  $\tilde{H}_{\text{pol,rfB}}$  in Eq. 7 and  $I$  is the identity operator. The eEDM coupling, as well as the detailed experimental sequence, for two molecules is discussed in the next section.

## II. DETAILS ON THE EXPERIMENTAL SEQUENCE AND DETECTION SCHEME

In this section we explain the experimental sequence by an example of an ideal experiment. The molecules are initialized in  $|0_{\downarrow}0_{\downarrow}\rangle$  via optical pumping and then entangled to  $\frac{1}{\sqrt{2}}(|0_{\uparrow}0_{\downarrow}\rangle - |0_{\downarrow}0_{\uparrow}\rangle)$ . An example protocol for entanglement generation is discussed in the next section. Next the molecule orientation is prepared in  $|\widetilde{\uparrow\downarrow}\rangle$  by a global  $\pi/2$ -pulse and a scalar light shift on one of the molecules, as described in the main text.

Since the total Hamiltonian for one molecule  $\tilde{H}_{\text{pol,rfB}}$  (Eq. 7) can be separated into two decoupled subspaces, we can reduce it to a  $2 \times 2$  matrix for each molecule orientation. For two molecules in  $|\widetilde{\uparrow\downarrow}\rangle$ , the total Hamiltonian in the basis of  $\{|\widetilde{\uparrow\uparrow}\rangle, |\widetilde{\uparrow\downarrow}\rangle, |\widetilde{\downarrow\uparrow}\rangle, |\widetilde{\downarrow\downarrow}\rangle\}$  is

$$H_{\uparrow\downarrow} = \frac{1}{2} \begin{pmatrix} 2\Omega_B & \omega_{\mathcal{P}} & \omega_{\mathcal{P}} & 0 \\ \omega_{\mathcal{P}} & 2\varepsilon_{\text{CPV}} & 0 & \omega_{\mathcal{P}} \\ \omega_{\mathcal{P}} & 0 & -2\varepsilon_{\text{CPV}} & \omega_{\mathcal{P}} \\ 0 & \omega_{\mathcal{P}} & \omega_{\mathcal{P}} & -2\Omega_B \end{pmatrix}. \quad (8)$$

The initial spin state in this basis is

$$|\Psi^-\rangle = \frac{1}{\sqrt{2}} \begin{pmatrix} 0 \\ +1 \\ -1 \\ 0 \end{pmatrix}. \quad (9)$$

Before turning on the magnetic field ( $\Omega_B = 0$ ), the eEDM spin precession is suppressed by the  $\omega_{\mathcal{P}}$  coupling in the triplet subspace. After turning on the magnetic field, as described in the main text,  $|\Psi^-\rangle$  is coupled by the eEDM interaction resonantly to the unshifted state

$$|u\rangle = \sin\theta|\Psi^+\rangle + \cos\theta|\Phi^+\rangle = \frac{1}{\sqrt{2}} \begin{pmatrix} \cos\theta \\ \sin\theta \\ \sin\theta \\ \cos\theta \end{pmatrix}, \quad (10)$$

with the mixing angle  $\theta$  given by  $\tan \theta = \Omega_B / \omega_P$ , and

$$|\Psi^+\rangle = \frac{1}{\sqrt{2}} \begin{pmatrix} 0 \\ 1 \\ 1 \\ 0 \end{pmatrix}, |\Phi^\pm\rangle = \frac{1}{\sqrt{2}} \begin{pmatrix} 1 \\ 0 \\ 0 \\ \pm 1 \end{pmatrix}. \quad (11)$$

The coupling strength is reduced to  $\varepsilon_u = 4\varepsilon_{\text{CPV}} \sin \theta$ .

After spin precession time  $T$ , the spin state is

$$\begin{aligned} |\psi\rangle &= \cos \varepsilon_u T |\Psi^-\rangle + i \sin \varepsilon_u T |u\rangle \\ &= \cos \varepsilon_u T |\Psi^-\rangle + i \sin \varepsilon_u T (\sin \theta |\Psi^+\rangle + \cos \theta |\Phi^+\rangle) = \frac{1}{\sqrt{2}} \begin{pmatrix} i \cos \theta \sin \varepsilon_u T \\ \cos \varepsilon_u T + i \sin \theta \sin \varepsilon_u T \\ -\cos \varepsilon_u T + i \sin \theta \sin \varepsilon_u T \\ i \cos \theta \sin \varepsilon_u T \end{pmatrix}. \end{aligned} \quad (12)$$

The magnetic field is turned off after an integer cycles of oscillations, when the lab basis coincides with the rotating frame basis, the spin state freezes in the lab frame (but starts to oscillate between  $|\Psi^+\rangle \leftrightarrow |\Phi^-\rangle$  in the rotating frame). After rotating the molecule orientation back to  $|00\rangle$ , the spin state remains the same. As a result,  $|\psi\rangle$  is the final spin state in the lab frame.  $|\psi\rangle$  is mostly  $|\Psi^-\rangle$ , because the eEDM spin precession phase is small, with a small admixture of  $|u\rangle$  (Eq. 10). The small difference between the initial ( $|\Psi^-\rangle$ ) and final ( $|\psi\rangle$ ) spin states in the lab frame indicates the eEDM spin precession phase.

To maximize the sensitivity, we need to measure in the  $\frac{1}{\sqrt{2}}(|\uparrow\downarrow\rangle \pm i|\downarrow\uparrow\rangle)$  basis, because  $|\Psi^-\rangle$  has equal projection on this set of basis states and the spin precession is in the same plane as the basis states. This is conceptually similar to rotating the phase of the spin or rotating the measurement basis by  $\pm\pi/4$  between spin initialization and measurement in conventional eEDM measurements to maximize the sensitivity to the spin precession [5]. Here, it can be achieved by two similar methods.

The first method works as follows. To start, we add an extra  $\pm\pi/2$  phase between  $|\uparrow\rangle$  and  $|\downarrow\rangle$  by a vector Stark shift [6] from an addressing beam on one of the molecules. The addressing beam on the second molecule shifting  $|\downarrow\rangle$  by  $\delta$ , as an example, is described by  $I \otimes \delta |\downarrow\rangle \langle\downarrow|$ . After a pulse time  $t$  with  $\delta t = \pi/2$ , the state  $|\psi\rangle$  becomes

$$\begin{aligned} |\psi'\rangle &= \cos \left( \frac{\pi}{4} + \varepsilon_u T \right) |\Psi^-\rangle + i \sin \left( \frac{\pi}{4} + \varepsilon_u T \right) \sin \theta |\Psi^+\rangle + i \frac{1}{\sqrt{2}} \sin \varepsilon_u T \cos \theta (|\Phi^+\rangle + i|\Phi^-\rangle) \\ &= \frac{1}{\sqrt{2}} \begin{pmatrix} i \cos \theta \sin \varepsilon_u T \\ i \cos \varepsilon_u T - \sin \theta \sin \varepsilon_u T \\ -\cos \varepsilon_u T + i \sin \theta \sin \varepsilon_u T \\ -\cos \theta \sin \varepsilon_u T \end{pmatrix}. \end{aligned} \quad (13)$$

$|\psi'\rangle$  now is roughly an equal superposition of  $|\Psi^-\rangle$  and a state in the triplet subspace. Next, we apply a global  $\pi$  rotation between  $|\uparrow\rangle \leftrightarrow |\downarrow\rangle$ . The singlet  $|\Psi^-\rangle$  is not coupled by global rotations. The  $|\Psi^+\rangle$  state is coupled to a superposition  $\cos \phi |\Phi^+\rangle + i \sin \phi |\Phi^-\rangle$ , where  $\phi$  is the phase of the global  $\pi$ -pulse, and the other superposition  $\cos \phi |\Phi^+\rangle - i \sin \phi |\Phi^-\rangle$  is a dark state. We choose a phase of  $-\pi/2$  (i.e.,  $-\sigma_y$  rotation), as a result, for the components in  $|\psi'\rangle$  (Eq. 13),  $\frac{1}{\sqrt{2}}(|\Phi^+\rangle + i|\Phi^-\rangle)$  is a dark state,  $|\Phi^+\rangle$  is mapped to  $\frac{1}{\sqrt{2}}(|\Phi^+\rangle - i|\Phi^-\rangle)$ , and  $|\Psi^-\rangle$  is uncoupled. The state after rotation for a small  $\varepsilon_u T$  ( $\sin \varepsilon_u T \approx \varepsilon_u T$  and  $\cos \varepsilon_u T \approx 1$ ) is

$$\begin{aligned} |\psi''\rangle &= \frac{1}{\sqrt{2}}(1 - \varepsilon_u T) |\Psi^-\rangle + i \frac{1}{2\sqrt{2}}(1 + (\sin \theta + \cos \theta)\varepsilon_u T) |\Phi^+\rangle + i \frac{1}{2\sqrt{2}}(1 + (\sin \theta - \cos \theta)\varepsilon_u T) |\Phi^-\rangle \\ &= \begin{pmatrix} i \frac{1}{\sqrt{2}}(1 + \varepsilon_u T \sin \theta) \\ \frac{1}{2}(1 - \varepsilon_u T) \\ -\frac{1}{2}(1 - \varepsilon_u T) \\ i \frac{1}{\sqrt{2}}\varepsilon_u T \cos \theta \end{pmatrix}. \end{aligned} \quad (14)$$

Finally, the populations are measured by fluorescence in  $|\uparrow\rangle$  and  $|\downarrow\rangle$ . The eEDM phase information is mapped to the parity of the population and we do not need single molecule resolved imaging. The population in the even and odd parity states are

$$\begin{aligned} P_{\uparrow\uparrow, \downarrow\downarrow} &= \frac{1}{2}(1 + \varepsilon_u T) \\ P_{\uparrow\downarrow, \downarrow\uparrow} &= \frac{1}{2}(1 - \varepsilon_u T) \end{aligned} \quad (15)$$

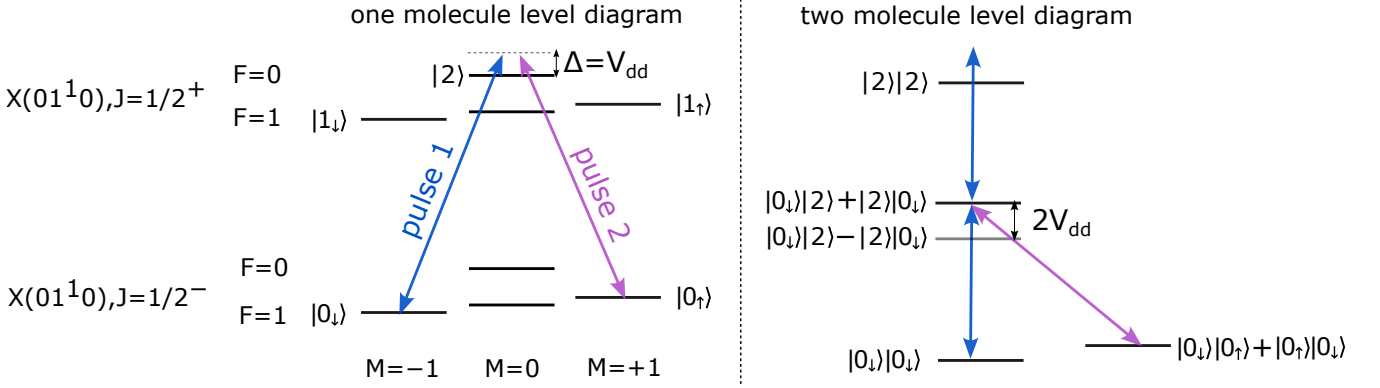


FIG. S2. Level diagram of a bending mode in a linear  $^2\Sigma$  molecule, for example YbOH [7–9]. We choose  $|X(01^10), J = 1/2^-, F = 1, M = \pm 1\rangle = |0_{\uparrow, \downarrow}\rangle$ ,  $|X(01^10), J = 1/2^+, F = 1, M = \pm 1\rangle = |1_{\uparrow, \downarrow}\rangle$ , and  $|X(01^10), J = 1/2^+, F = 0, M = 0\rangle = |2\rangle$ .  $|0_{\uparrow}\rangle$  and  $|2\rangle$  are connected by an electric dipole transition and the pair states  $\frac{1}{\sqrt{2}}(|0_{\downarrow}2\rangle \pm |20_{\downarrow}\rangle)$  and they are split by  $2V_{dd}$ . Rf pulse 1 (blue arrows) couples  $|0_{\downarrow}\rangle \leftrightarrow |2\rangle$  and pulse 2 (purple arrows) couples  $|2\rangle \leftrightarrow |0_{\uparrow}\rangle$  with the same detuning  $\Delta = V_{dd}$ . A magnetic field is applied to split the Zeeman sublevels during entanglement generation.

An alternative detection method, similar to the one described above, is to apply a  $\pi$  pulse on two molecules with different phases on the state  $|\psi\rangle$  (Eq. 12) and measure the parity. For instance, if we apply  $-\sigma_y \otimes I + I \otimes \sigma_x$ , the  $\frac{1}{\sqrt{2}}(|\uparrow\downarrow\rangle + i|\downarrow\uparrow\rangle)$  state is mapped to the even parity states ( $|\uparrow\uparrow\rangle, |\downarrow\downarrow\rangle$ ) while the  $\frac{1}{\sqrt{2}}(|\uparrow\downarrow\rangle + i|\downarrow\uparrow\rangle)$  remains in the odd parity states ( $|\uparrow\downarrow\rangle, |\downarrow\uparrow\rangle$ ), which can be distinguished by fluorescence detection. This method requires the ability to perform single molecule-resolved rotation, which can be achieved by a two-photon transition with focused lasers. An advantage compared to the first method is that the phase of the measurement basis is set by the phase of the laser field, but not the intensity of the addressing beam. Both methods together may be used for checking systematic effects, and even in parallel in systems with multiple pairs of molecules.

### III. ROBUSTNESS TO EXPERIMENTAL IMPERFECTIONS

Our scheme is robust to various experimental imperfections. For example, the fidelity of entanglement generation does not have a lower threshold; the population that is not initialized in  $|\Psi^-\rangle$  is not coupled by the eEDM and only contributes a constant background. The optimal scheme with imperfect entanglement generation is discussed in Sec. VI. Many possible sources may cause imperfect initialization of the molecule orientation; they include, for instance, fluctuations in the  $\pi/2$ -pulse power, Stark shifts, imperfect single molecule addressing light shift, or small difference in the  $g$ -factors of  $|0\rangle$  and  $|1\rangle$  states (resulting from perturbations of other electronic states), etc. If a molecule is not in equal superposition of  $|0\rangle$  and  $|1\rangle$  the eEDM interaction ( $\Sigma_0$ ) is slightly reduced. If two molecules are not in exact opposite phases of  $|0\rangle$  and  $|1\rangle$  superpositions, the splitting between  $|\uparrow\downarrow\rangle$  and  $|\downarrow\uparrow\rangle$  is reduced (this can be used as a switch to tune the spin precession rate). If two molecules have different  $|0\rangle$  and  $|1\rangle$  populations, their eEDM interactions ( $\Sigma_0$ ) are different and thus  $|\Psi^-\rangle$  is also coupled to the  $|\Phi^\pm\rangle$  states. However, this additional coupling does not cause spin precession since the  $|\Phi^\pm\rangle$  states are strongly coupled by the magnetic field (see Fig. 2[c] in the main text). Importantly, all the fields are applied independently and they do not have correlation with the eEDM switch (AC Stark shift from the addressing beam). As a consequence, these imperfections do not lead to systematic effects directly, but instead to contrast reduction and increased statistical noise.

Magnetic field correlated rf electric fields, stray electric fields, and black-body radiation (BBR) have detrimental effects on the state of molecule orientation and need to be shielded. Our scheme does not require a DC electric field, and shielding electric fields is straightforward, especially without the need for electric field plates nearby. The effects of the residual fields include near-resonant couplings between  $|0\rangle \leftrightarrow |1\rangle$  and off-resonant effects, such as energy shifts on  $|0\rangle$  and  $|1\rangle$ . The coupling effect is suppressed by the dipole-dipole interaction between two molecules when the residual-field coupling strength is weaker than the dipole-dipole interaction (typically  $\sim$  kHz at  $\sim \mu\text{m}$  separation), and it can also be mitigated by applying a stronger electric field in phase with the molecule oscillation.

Stray electric fields or off-resonance BBR can cause an energy shift between  $|0\rangle$  and  $|1\rangle$ . This alters the oscillating frequency of the rotating molecules, which may affect coherent control of the molecule orientation and may interfere with the eEDM spin precession by shifting the oscillation out of phase with the magnetic rf field. Nevertheless, stray

electric fields can be actively measured and cancelled, especially since the molecules needed for this protocol will be trapped in a small volume  $\sim \text{mm}^3$ ; for example, in trapped ions a residual electric field lower than 0.1 mV/cm has been achieved [10, 11]. A 0.1 mV/cm fluctuation corresponds to a maximum  $\sim 50$  MHz dephasing rate for a molecule of  $d_0 \approx 2$  D dipole moment and  $\omega_P \approx 100$  kHz parity splitting. This leads to a coherence time of  $\sim 10$  s, and the coherence time is inversely proportional to parity splitting. On the other hand, we need  $\Omega_B \approx \mu_B g B \gtrsim 2\omega_P$ , where  $g$  is the electron magnetic  $g$ -factor. To avoid using high magnetic field (a few Gauss, using a similar magnetic field coil setup in ref. [12]), our scheme is most suitable for molecules with  $\omega_P \lesssim 10$  MHz, which is a typical range for parity doubling. In addition, for trapped ions,  $\omega_P$  needs to be much lower than the trap rf frequency ( $\sim 20$  MHz). Some examples of suitable neutral and ion species are listed in the Supplemental Material.

#### IV. AN EXAMPLE OF ENTANGLEMENT GENERATION

As mentioned in the main text, the spin entangled initial state  $\frac{1}{\sqrt{2}}(|0_\uparrow 0_\downarrow\rangle - |0_\downarrow 0_\uparrow\rangle)$  can be prepared by existing entanglement protocols together with single molecule rotations. Here we present an example for the YbOH molecule, which is the only molecule for which the parity-doubled bending mode has been completely mapped out [8]. Note that the level structures for other metal hydroxide molecules (SrOH, CaOH, RaOH, etc) are similar and therefore the same experimental sequence can be applied. More generally, a similar entanglement sequence can be found for any polar molecules using the dipole-dipole interaction or other types of interactions.

The level diagram of the YbOH molecule is shown in Fig. S2. We propose to use the  $X(01^1 0)$ ,  $J = 1/2^-$ ,  $F = 1$ ,  $M = \pm 1$  states as  $|0_\uparrow\rangle$  and  $|0_\downarrow\rangle$  states, and use  $X(01^1 0)$ ,  $J = 1/2^+$ ,  $F = 1$ ,  $M = \pm 1$  states as  $|1_\uparrow\rangle$  and  $|1_\downarrow\rangle$  states. The  $|0\rangle$  and  $|1\rangle$  states are separated by  $\sim 35$  MHz for YbOH [8], and similarly for other metal hydroxide molecules. We list the parity splitting of other types of molecules in Sec. VII. Note that tensor light shifts have negligible effect on the coherence between spin states (i.e.,  $\uparrow$  and  $\downarrow$  are shifted by the same frequency), and have negligible effect on coherence between the opposite parity states. This is because the opposite parity states have similar transition dipole moments to the excited states and the transition frequencies are different by the parity splitting order of magnitude (typically between 100 kHz and 100 MHz), which is suppressed by the large detuning (typically  $\sim 100$  THz) of the trapping light. A magnetic field is applied to split the Zeeman sublevels during entanglement generation. We choose another state  $X(01^1 0)$ ,  $J = 1/2^+$ ,  $F = 0$ ,  $M = 0$ , labeled as  $|2\rangle$ , as an ancillary state for the entanglement generation.  $|2\rangle$  can be any state that is connected with  $|0_\downarrow\rangle$  by an electric dipole transition. The dipole-dipole interaction between  $|0_\downarrow 2\rangle \leftrightarrow |20_\downarrow\rangle$  is  $V_{dd}$ , which depends on the transition dipole moment and the distance between two molecules. For molecules with  $\sim 2$  Debye molecule frame dipole moment and  $\sim \mu\text{m}$  separation,  $V_{dd}$  is around 100 kHz. The eigenstates of the dipole-dipole interaction are  $\frac{1}{\sqrt{2}}(|0_\downarrow 2\rangle \pm |20_\downarrow\rangle)$  and they are split by  $2V_{dd}$ .

Two molecules are initialized in  $|0_\downarrow 0_\downarrow\rangle$  by optical pumping. An rf pulse coupling  $|0_\downarrow\rangle \leftrightarrow |2\rangle$  with a detuning  $\Delta = V_{dd}$  is applied. This pulse resonantly couples the pair states  $|0_\downarrow 0_\downarrow\rangle \leftrightarrow \frac{1}{\sqrt{2}}(|0_\downarrow 2\rangle + |20_\downarrow\rangle)$ , and off-resonantly couples  $\frac{1}{\sqrt{2}}(|0_\downarrow 2\rangle + |20_\downarrow\rangle) \leftrightarrow |22\rangle$ . If the coupling Rabi frequency is much less than  $V_{dd}$ , only the entangled state  $\frac{1}{\sqrt{2}}(|0_\downarrow 2\rangle + |20_\downarrow\rangle)$  is populated after a  $\pi$  pulse (the pulse area is  $\pi/\sqrt{2}$  for a single molecule). Next, another pulse coupling  $|2\rangle \leftrightarrow |0_\uparrow\rangle$  with a detuning  $\Delta = V_{dd}$  is applied. Note that the first and second pulses can be different in polarization or frequency, so the first pulse does not drive the  $|2\rangle \leftrightarrow |0_\uparrow\rangle$  transition. After a  $\pi$  pulse (the pulse area is  $\pi$  for a single molecule), the population in  $|2\rangle$  is mapped to  $|0_\uparrow\rangle$  for each molecule and the pair state is  $\frac{1}{\sqrt{2}}(|0_\uparrow 0_\downarrow\rangle + |0_\downarrow 0_\uparrow\rangle)$ . Subsequently, a  $\pi$  phase can be added on the  $|0_\downarrow 0_\uparrow\rangle$  component by the vector Stark shift of an addressing beam focusing on one of the molecules. The entangled state  $\frac{1}{\sqrt{2}}(|0_\uparrow 0_\downarrow\rangle - |0_\downarrow 0_\uparrow\rangle)$  is prepared.

Next, the DC magnetic field is switched off, and as described in the main text, a  $\pi/2$  pulse  $|0\rangle \leftrightarrow |1\rangle$  is applied to both molecules. They are prepared in  $\uparrow\uparrow$ , and an AC Stark shift by an addressing beam focusing on one of the molecules is applied to shift the phase of  $|1_{\uparrow,\downarrow}\rangle$  by  $\pi$ . The state is prepared in  $\uparrow\downarrow$ . Then an rf magnetic field is turned on and spin precession starts. After spin precession, the eEDM phase shift is measured by the sequence described in the previous section.

After spin precession, we use the methods described in the previous section to measure the phase shift from the eEDM interaction.

#### V. SCALING UP TO $2N$ MOLECULES

For  $2N$  molecules, the eEDM sensitivity increases linearly as the molecule number (Heisenberg scaling). We explain the scaling in Fig. S3. Since the eEDM interaction is diagonal in the  $\otimes_{2N}\{|\uparrow\rangle, |\downarrow\rangle\}$  basis (see Eq. 5), it does not flip spins and it shifts the two states  $|\widetilde{\uparrow\downarrow\uparrow\dots}\rangle$  and  $|\widetilde{\downarrow\uparrow\downarrow\dots}\rangle$  oppositely. As a result, the eEDM causes spin precession

within the two dimensional subspace of  $\{|\widetilde{\uparrow\uparrow\uparrow\dots}\rangle, |\widetilde{\downarrow\downarrow\downarrow\dots}\rangle\}$ . Since these two states form a two-dimensional subspace spanned by  $|S = N, S_z = 0\rangle$  and  $|S = 0, S_z = 0\rangle$ , the eEDM interaction will not couple them to any other states. The entangled state of  $2N$  molecules may be generated by adiabatic sweeping to the many-body ground state, which has been demonstrated in Rydberg atom systems [13], or using universal gate operations. These methods requires longer time for entangling larger systems. In addition, the entangled state may be generated by measurement and feedback on a cluster state [14–17], which can be generated by parallel operations. This method has a constant circuit depth for arbitrary numbers of entangled molecules. Once the molecules are entangled, the qubit states can be mapped to the spin states.

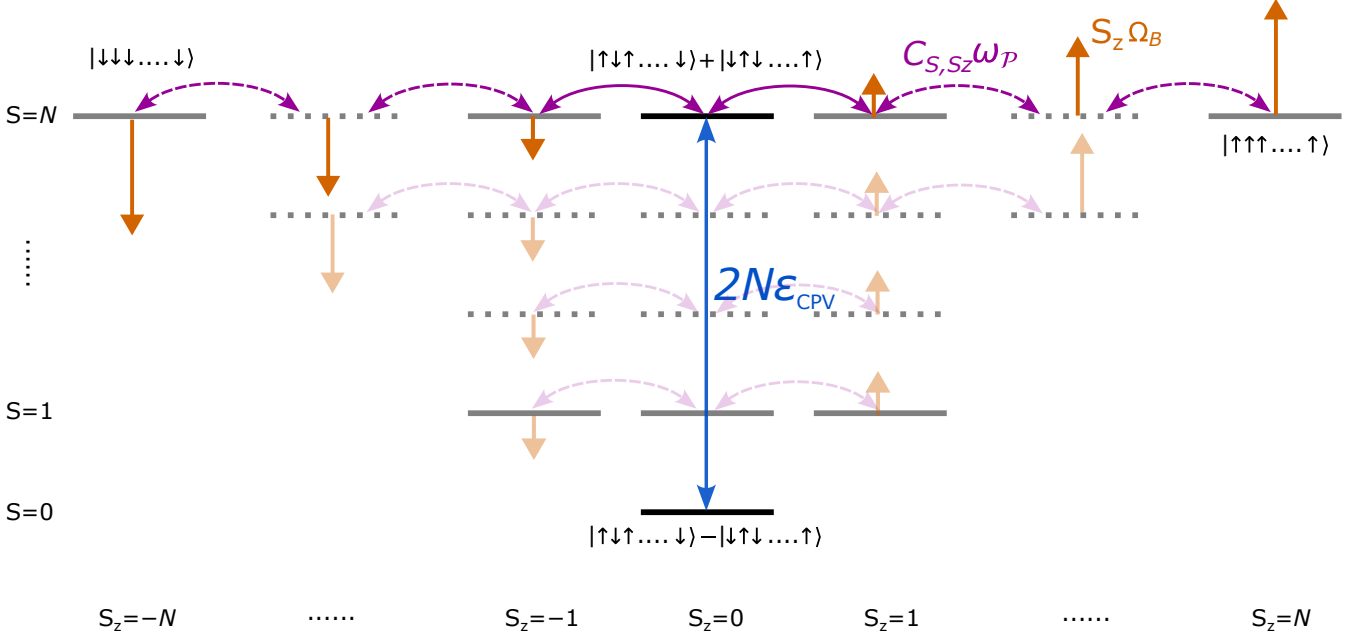


FIG. S3. For  $2N$  molecules with oppositely aligned molecule orientations, the spin states can be described by the Dicke ladder. The vertical dimension is ordered by total spin and the horizontal dimension is ordered by the spin projection on the quantization axis. In the rotating frame, the eEDM interaction couples the  $|S = 0, S_z = 0\rangle \leftrightarrow |S = N, S_z = 0\rangle$  (blue arrow). Similar to the two molecule case, the  $S = N$  subspace is coupled by the rotation of the reference frame (purple arrows), the parameter  $C_{S,S_z}$  is given by the Clebsch-Gordan coefficients. We apply an rf magnetic field, which shifts the energies of states with nonzero  $S_z$ . Similar to the two molecule case, the magnetic field and the rotation together gives an unshifted state with most population in  $|S = N, S_z = 0\rangle$ .

## VI. OPTIMAL MEASUREMENT SCHEMES FOR SYSTEMS WITH FINITE ERROR PROBABILITIES

In earlier sections, we have explained the measurement scheme in the maximal limit, where all  $M = 2N$  molecules are prepared with perfect fidelity into the entangled spin states. In this idealized limit, the spin states that have the maximum eEDM coupling (sensitivity) are the antiferromagnetic (AFM)-GHZ states  $|\text{AFM}_{\pm}\rangle = |\uparrow\downarrow\uparrow\dots\downarrow\rangle \pm |\downarrow\uparrow\downarrow\dots\uparrow\rangle$ , which reduce to  $|\text{AFM}_{\pm}\rangle = \Psi^{\pm}$  in the two-molecule case. In a real implementation, however, finite error probabilities will reduce the size of the AFM state that provides optimal metrological gain to  $2N < M$ .

In this section, we show how to optimize the eEDM sensitivity gain for systems with finite gate errors. We assume that the initial state is prepared in  $|\text{AFM}_{-}\rangle$  with a multipartite entanglement fidelity of  $F_{\text{total}}$ . The definition of  $F_{\text{total}}$  is given by the average of the population in the  $|\uparrow\downarrow\uparrow\dots\downarrow\rangle$  and  $|\downarrow\uparrow\downarrow\dots\uparrow\rangle$  components and the coherence between them [18]. The eEDM interaction couples  $|\text{AFM}_{-}\rangle \leftrightarrow |\text{AFM}_{+}\rangle$  and is measured in the end by mapping the  $|\text{AFM}_{+}\rangle$  state to the normal GHZ states by a global rotation on all spins (see previous sections). As Eq. (13-14) indicates, the population that can be rotated and subsequently measured is limited by the population and the coherence of  $|\uparrow\downarrow\uparrow\dots\downarrow\rangle$  and  $|\downarrow\uparrow\downarrow\dots\uparrow\rangle$  components, which coincides with the multipartite entanglement fidelity  $F_{\text{total}}$ . As a result, the metrological sensitivity in an imperfect experiment using  $2N$  molecules is  $2NF_{\text{total}}$ . The relative gain compared to the non-entangled metrology (standard quantum limit [SQL]) is  $2NF_{\text{total}}/\sqrt{2N} = \sqrt{2N}F_{\text{total}}$ . When  $\sqrt{2N}F_{\text{total}} > 1$ , the eEDM measurement benefits from quantum-enhanced metrology.



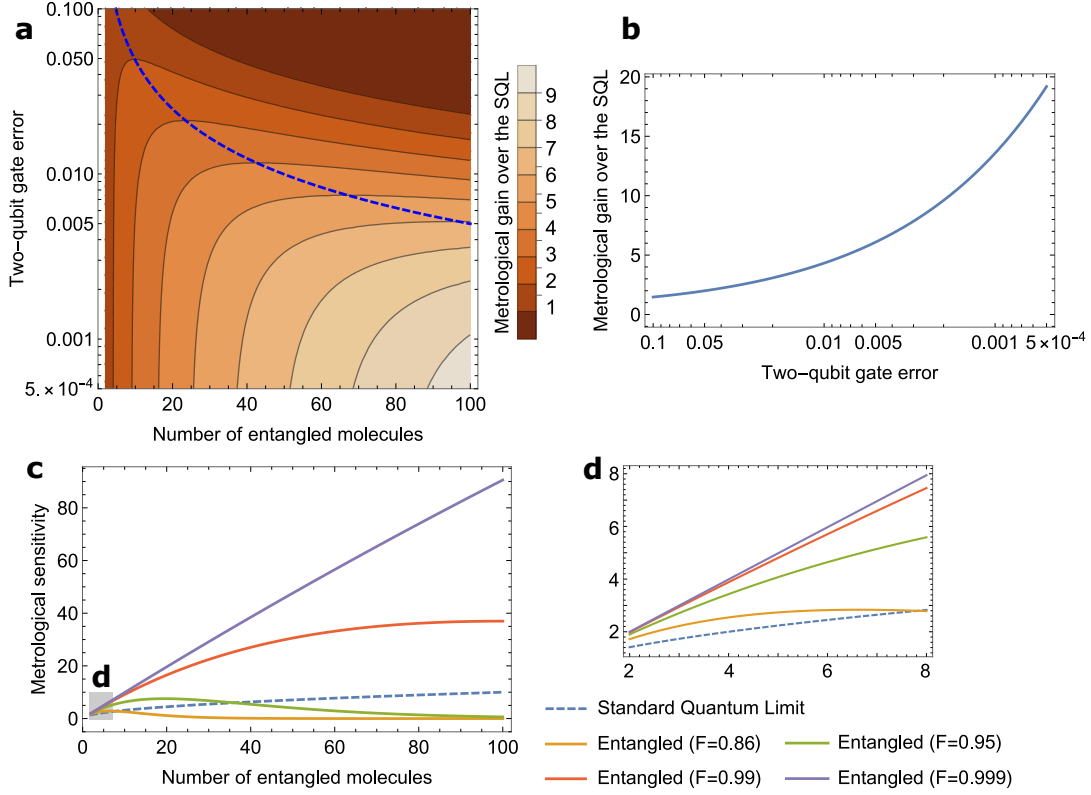


FIG. S4. (a). The enhancement of the metrological sensitivity using the entangled scheme over non-entangled scheme (SQL). The blue dashed line shows the optimal number of entangled molecule as a function of two-molecule gate fidelity (b). For a given total number of molecule, the optimal enhancement of the metrological gain over the SQL as a function of the two-molecule gate fidelity. (c) and (d). Comparison of the metrological sensitivities of the imperfect entangled scheme ( $F$  in the legend is the two-molecule entangling gate fidelity) and the SQL. (d) is a zoom-in of (c). Note that  $F = 0.86$  and  $F = 0.87$  have already been achieved in initial demonstrations of two-molecule entanglement [20, 21].

The multipartite entanglement fidelity  $F_{\text{total}}$  depends on both the molecule number ( $2N$ ) and the two-particle entangling gate fidelity ( $F$ ). In the simplest case, we can perform two-molecule gate ([19–21]) operations  $2N - 1$  times to generate the  $2N$  molecule entanglement with linear time overhead, which for small  $N$  is negligible compared to molecule coherence times presently demonstrated [22, 23]. For large  $N$  (where the linear time-cost approaches the coherence time), constant time methods that involve  $2(2N - 1)$  parallel gate operations can be used with a constant  $F^2$  reduction to the overall state fidelity [14–17]. Since the single-molecule rotation error is negligible compared to the two-particle gates, we have  $F_{\text{total}} \approx F^{(2N-1)}$  for the linear time-overhead approach. Thus, for a system of  $M$  molecules divided into  $M/2N$  partitions, where in each partition  $2N$  molecules are entangled, the total metrological gain over the SQL is  $\sqrt{2N}F^{(2N-1)}$ . (We mention in passing that in experiments limited by technical noise rather than the SQL, the suppression of susceptibility to external field noise, which we do not discuss in this section, further enhances the measurement sensitivity beyond the improvements given by the SQL gain factor.)

Fig. S4(a) and (b) show the enhancement of metrological gain over the SQL as a function of the size of the entanglement (number of molecules entangled) and the fidelity of two-molecule entangling gate error. Fig. S4(c) and (d) directly compare the metrological sensitivities of the entangled scheme (thick lines) with the standard quantum limit (dashed line) for several different choices of two-molecule entangling gate fidelity. At the entanglement fidelities achieved in Ref. [20] ( $F = 0.86$ ) and [21] ( $F = 0.87$ ), the scaling indicates an optimal advantage at 4 entangled molecules, or  $2N \approx -1/(2 \log(F))$  for general cases of  $F$ . As depicted by Fig. S4(c) and (d), the maximum metrological gain over the SQL,  $F^{(-1/(2 \log F) - 1)} \sqrt{-1/(2 \log F)}$ , scales quasi-polynomially with future improvements [24] to two-molecule gate fidelities.

Intuitively, the emergence of an optimal entangled system size can be interpreted as the competition between the linear gain and the exponential decay of the “correlation length” of the AFM order. Experimental imperfections reduces the quantum correlation between distant spins, and thus the two uncorrelated spins may counteract each other’s contribution to the eEDM coupling. In analogy to an uncorrelated, sequential measurement, the optimal

interrogation time for a single measurement is around the coherence time of the system, within which the sensitivity increases linearly with respect to the interrogation time prior to exponential decay in the signal contrast.

## VII. MOLECULAR DESIGN REQUIREMENTS

As discussed in the main text, the entangled-basis eEDM couplings are maximal when the molecular dipole oscillations – set by the opposite-parity splitting  $\omega_P$  – are adiabatic relative to the RF magnetic field drive  $\Omega_B$ . Limiting RF  $B$ -fields to achievable amplitudes therefore imposes upper bounds on the size of the parity splitting  $\omega_P$  relative to the magnetic tuning of the molecule. Conversely, stray-field considerations also impose a lower bound on the minimum parity doubling to avoid excess decoherence and accidental polarization. RF drives on trapped ions must additionally be well-separated from trap frequencies ( $\sim 20$  MHz).

In rigid-rotor molecules, the most generic parity splitting scale is set by the end-to-end rotation, which is inversely proportional to the largest rotational moment of inertia. For small molecules, typical end-to-end rotational scales are several GHz. While far-detuned from typical ion trapping frequencies, these splittings impose demanding requirements on RF  $B$ -field intensities (e.g.  $> 500$  G for a paramagnetic  $^2\Sigma$  molecule). Achieving sub-GHz end-to-end rotation is possible, but requires molecules with both heavy metal and ligand partners [25–27].

Technical requirements on  $B$ -field amplitudes can be significantly relaxed, however, by using molecules with near-degenerate parity doubling, for which typical  $\omega_P$  splittings are  $< 100$  MHz. A standard approach is to utilize states with non-zero orbital angular momentum ( $\Lambda > 0$ ), which form near-degenerate  $\Omega$ -doublets of combined electronic and rotational angular momenta. These states can be found in the electronic configurations of linear diatomic molecules, where the relevant quantum numbers include orbital angular momentum projection onto the molecular axis ( $\Lambda$ ), electron spin angular momentum projection on the molecular axis ( $\Sigma$ ), and the sum of these projection quantum numbers ( $\Omega$ ). To facilitate the RF magnetic drive, it is furthermore desirable to utilize the stretched states with maximal  $|\Omega|$ , where there are no cancellations to magnetic sensitivity from mixed orientations of orbital and electron spin angular momenta.

Note that this is opposite to the design considerations in some contemporary eEDM experiments, where the non-stretched  $^3\Delta_1$  configuration is utilized for measurements due to its suppressed  $g$ -factor [28, 29]. In our scheme, the antiferromagnetic ordering of the entangled states already confers insensitivity to global magnetic field noise, which in combination with immunity to slow noise from the rotating frame, significantly reduces the technical need for a magnetically insensitive state. If local magnetic insensitivity (or a diamagnetic molecule) were desired, however, one could alternatively perform the effective RF  $B$ -field via two-photon E1 drives to a magnetic, excited electronic state or amplitude-modulated AC light shifts. However, this merely shifts the experimental susceptibility to magnetic noise onto laser power and polarization noise; whether this approach is indeed advantageous depends on details of the technical implementation.

Operating under the assumption that a magnetic state is desired, we note that states with larger values of  $|\Omega|$  are coupled at progressively higher orders and therefore exhibit smaller  $\Omega$ -doubling and  $\omega_p$ . As discussed earlier, an excessively small or unresolved  $\omega_p$  decreases the protection conferred by the rotating frame (because it is slow) and risks accidental polarization from stray electric fields. Table S1 lists the leading  $\Omega$ -doubling mechanisms and matrix element scales with respect to electronic ( $\Delta E$ ), spin-orbit ( $A$ ), and rotational ( $B$ ) splittings for a variety of open-shell, non-zero  $\Lambda$  and  $\Omega$  electronic configurations, which can be utilized for order-of-magnitude estimates of  $\omega_p$  for molecules with  $\Omega$ -doubled electronic configurations. Imposing the additional constraint that eEDM-sensitive states must have non-zero spin projection on the molecular axis ( $\Sigma \neq 0$ ), we find that  $^2\Pi_{3/2}$  and  $^4\Delta_{1/2}$  states are most likely to meet the requirements for  $\sim \mu_B$  magnetic tuning and kHz to MHz-scale parity-splitting  $\omega_p$ . These electronic configurations can be found in a range of EDM-sensitive molecular ions, several of which are listed in table S3.

An even more flexible approach to engineering parity doublets is to rely on near-degeneracies that originate from rovibrational, rather than orbital electronic degrees of freedom, which are present universally in polyatomic (more than two atom) molecules. This provides the added advantage of decoupling polarization from the choice of metal center – a feature which is particularly useful for neutral molecules, where the metal center can be designed to be compatible with optical cycling and laser cooling, as well as for integrating exotic rare isotopes (with arbitrary electronic structure) into parity-doubled neutral and ionic molecules. Common structural motifs [7, 30, 31] for engineering rovibrational doublets include linear molecules with bending-induced  $\ell$ -doubling (e.g. linear MOH) as well as non-linear symmetric (e.g. MCH<sub>3</sub>) and asymmetric tops (e.g. planar MNH<sub>2</sub>, bent MSH) with rotationally induced  $K$ -doubling. Control and trapping of eEDM-sensitive polyatomics is being actively pursued across several experiments and molecular species. In table S2, we list several common rovibrational doubling mechanisms and scales in polyatomic molecules. Specific polyatomic typologies are listed in Table S3.

State	Interactions	Effective form	Scaling	Prefactors	$\omega_p$ (approx.)
$^2\Pi_{1/2}$	$H_{L+} \times H_{so}$	$J_+ S_+ + J_- S_-$	$\frac{B(A)}{\Delta E}$	$2 \times (J + \frac{1}{2})$	$\sim 1 - 10$ GHz
$^2\Pi_{3/2}$	$(H_{L+})^2 \times H_{S+}$	$J_+^3 + J_-^3$	$\frac{B^3}{A(\Delta E)}$	$6 \times \prod_{i=-1/2}^{3/2} (J+i)$	$\sim 10 - 100$ Hz
$^3\Pi_1$	$(H_{L+})^2$	$J_+^2 + J_-^2$	$\frac{B^2}{\Delta E}$	$2 \times J(J+1)$	$\sim 0.1 - 1$ MHz
$^3\Pi_2$	$(H_{L+})^2 \times (H_{S+})^2$	$J_+^4 + J_-^4$	$\frac{B^4}{A^2(\Delta E)}$	$24 \times \prod_{i=-1}^2 (J+i)$	$\sim 10 - 100$ mHz
$^2\Delta_{3/2}$	$(H_{L+})^3 \times H_{so}$	$J_+^3 S_+ + J_-^3 S_-$	$\frac{B^3 A}{\Delta E^3}$	$6 \times \prod_{i=-1/2}^{3/2} (J+i)$	$\sim 1 - 10$ Hz
$^2\Delta_{5/2}$	$(H_{L+})^4 \times H_{S+}$	$J_+^5 + J_-^5$	$\frac{B^5}{A(\Delta E)^3}$	$120 \times \prod_{i=-3/2}^{5/2} (J+i)$	$< 10$ mHz
$^3\Delta_1$	$(H_{L+})^2 \times (H_{so})^2$	$J_+^2 S_+^2 + J_-^2 S_-^2$	$\frac{B^2 A^2}{\Delta E^3}$	$24 \times J(J+1)$	$\sim 0.1 - 1$ MHz
$^3\Delta_2$	$(H_{L+})^4$	$J_+^4 + J_-^4$	$\frac{B^4}{\Delta E^3}$	$24 \times \prod_{i=-1}^2 (J+i)$	$\sim 1 - 10$ mHz
$^3\Delta_3$	$(H_{L+})^4 \times (H_{S+})^2$	$J_+^6 + J_-^6$	$\frac{B^6}{A^2(\Delta E)^3}$	$720 \times \prod_{i=-2}^3 (J+i)$	$< 10$ mHz
$^4\Delta_{1/2}$	$H_{L+} \times (H_{so})^3$	$J_+ S_+^3 + J_- S_-^3$	$\frac{A^3 B}{\Delta E^3}$	$24 \times (J + \frac{1}{2})$	$\sim 0.1 - 1$ GHz
$^2\Phi_{5/2}$	$(H_{L+})^5 \times H_{so}$	$J_+^5 S_+ + J_-^5 S_-$	$\frac{B^5 A}{\Delta E^5}$	$720 \times \prod_{i=-3/2}^{5/2} (J+i)$	$< 10$ mHz
$^2\Phi_{7/2}$	$(H_{L+})^6 \times H_{S+}$	$J_+^7 + J_-^7$	$\frac{B^6}{A(\Delta E)^4}$	$720 \times \prod_{i=-5/2}^{7/2} (J+i)$	$< 10$ mHz
$^4\Phi_{3/2}$	$(H_{L+})^3 \times (H_{so})^3$	$J_+^3 S_+^3 + J_-^3 S_-^3$	$\frac{B^3 A^3}{\Delta E^5}$	$720 \times \prod_{i=-1/2}^{3/2} (J+i)$	$\sim 1 - 100$ Hz

TABLE S1. Orbital parity-doubling mechanisms and approximate  $\omega_p$  scales for heavy, spin-orbit-coupled molecules. Listed are  $\Omega$ -doubling matrix elements (at the single-configuration level) of selected  $C_{\infty v}$  electronic terms ( $^{2S+1}\Lambda_{\Omega}$ ). The  $H_{L+}$ ,  $H_{S+}$ , and  $H_{so}$  interactions refer to  $L$ -uncoupling ( $J \cdot L$ ),  $S$ -uncoupling ( $J \cdot S$ ), and microscopic spin-orbit ( $\sum_i l_i \cdot s_i$ ) terms, respectively. In the “scaling” column, the terms  $B$ ,  $A$ , and  $\Delta E$  refer to the rotational constant, spin-orbit constant, and electronic bandgaps to the perturbing level. Numerical prefactors are given by the product of  $n!$  coupling paths for an  $n$ -th order perturbation and factors of  $\sqrt{J(J+1)}$  from evaluating  $J^{+/-}$  terms in the effective Hamiltonians. The size of  $\omega_p$  for lowest- $J$  states are estimated assuming  $A \sim 4 \times 10^3$  cm $^{-1}$ ,  $\Delta E \sim 2 \times 10^4$  cm $^{-1}$ , and  $B \sim 0.2$  cm $^{-1}$ , which provides rough values for the scale of typical single-configuration, single-perturber contributions to the  $\Omega$ -doubling. Full computation of the  $\Omega$ -doubling splittings is highly species-dependent and usually involves complicated sums over multiple perturbing channels and electronic state configurations, which can exhibit cancellations and contributions that are not accounted for in these simplified estimates.

Type	Mechanism(s)	Doublet Quanta	$\omega_p$ (typ.)
rotation-vibration	centrifugal distortion	$l, K$	$< 10$ MHz
	inertial asymmetry	$K_a$	
anisotropic	spin-dipolar ( $S \cdot I$ )	$l, K, K_a$	$1 - 10$ MHz
electron hyperfine	spin-rotation ( $S \cdot N$ )	$l, K, K_a$	
anisotropic	spin-dipolar ( $I_i \cdot I_j$ )	$l, K, K_a$	$1 - 10$ kHz
nuclear hyperfine	spin-rotation ( $I \cdot N$ )	$l, K, K_a$	

TABLE S2. Common rovibrational parity-doubling mechanisms and splitting scales in polyatomic molecules.

Class	Species	Science State	$\omega_p$
rigid-rotor	alkaline-earth monofluorides (e.g. YbF [32, 33], BaF [34, 35], RaF [36–38])	$^2\Sigma^+$	$\sim 5$ GHz
	assembled alkaline-earth coinage (e.g. RaAg, RaAu [25–27])		$\sim 500$ MHz
$\Omega$ -doubled	$\Lambda = 1$ diatomics (e.g. PbF [39–41], BiF $^+$ )	$^2\Pi_{3/2}$	$\sim 10 - 100$ Hz
	$\Lambda = 2$ diatomics (e.g. IrF $^+$ , PtO $^+$ )	$^4\Delta_{1/2}$	$\sim 100$ MHz
	$C_{\infty v}$ linear (e.g. MOH [8])	$^2\Sigma^+(v_{\text{bend}}, \ell > 0)$	$\sim 20$ MHz
polyatomics	$C_{(n \geq 3)v}$ symmetric (e.g. MOCH $_3$ [31])	$^2A_1$ ( $K > 0$ )	$\sim 100$ kHz
	$C_{2v}$ planar asymmetric (e.g. MNH $_2$ [30])	$^2A_1$ ( $K_a > 0$ )	$\sim 1$ MHz
	$C_s, C_1$ bent asymmetric/chiral (e.g. MSH [30])	$^2A'$ ( $K_a > 0$ )	$\sim 5$ MHz

TABLE S3. Examples of paramagnetic EDM-sensitive molecules, science state configurations, and approximate parity splitting scales  $\omega_p$ , based on the scaling relations described in the text and figs. S1 and S2. Molecules listed without references have not, to our knowledge, been previously considered in the literature. Electronic configurations are inferred from periodic trends and comparison to iso-electronic systems.

- 
- [1] A. Petrov and A. Zakharova, Sensitivity of the yboh molecule to  $\mathcal{PT}$ -odd effects in an external electric field, *Phys. Rev. A* **105**, L050801 (2022).
  - [2] M. Borkowski, L. Reichsöllner, P. Thekkeppatt, V. Barbé, T. van Roon, K. van Druten, and F. Schreck, Active stabilization of kilogauss magnetic fields to the ppm level for magnetoassociation on ultranarrow feshbach resonances (2023), 2303.13682 [physics].
  - [3] P. Yu and N. R. Hutzler, Probing Fundamental Symmetries of Deformed Nuclei in Symmetric Top Molecules, *Phys. Rev. Lett.* **126**, 023003 (2021).
  - [4] M. Verma, A. M. Jayich, and A. C. Vutha, Electron electric dipole moment searches using clock transitions in ultracold molecules, *Phys. Rev. Lett.* **125**, 153201 (2020).
  - [5] J. Baron, W. C. Campbell, D. DeMille, J. M. Doyle, G. Gabrielse, Y. V. Gurevich, P. W. Hess, N. R. Hutzler, E. Kirilov, I. Kozyryev, B. R. O’Leary, C. D. Panda, M. F. Parsons, B. Spaun, A. C. Vutha, A. D. West, and E. P. West, Methods, analysis, and the treatment of systematic errors for the electron electric dipole moment search in thorium monoxide, *New J. Phys.* **19**, 073029 (2017).
  - [6] L. Caldwell and M. R. Tarbutt, General approach to state-dependent optical-tweezer traps for polar molecules, *Phys. Rev. Res.* **3**, 013291 (2021).
  - [7] I. Kozyryev and N. R. Hutzler, Precision measurement of time-reversal symmetry violation with laser-cooled polyatomic molecules, *Phys. Rev. Lett.* **119**, 133002 (2017).
  - [8] A. Jadbabaie, Y. Takahashi, N. H. Pilgram, C. J. Conn, Y. Zeng, C. Zhang, and N. R. Hutzler, Characterizing the fundamental bending vibration of a linear polyatomic molecule for symmetry violation searches (2023).
  - [9] Y. Takahashi, C. Zhang, A. Jadbabaie, and N. R. Hutzler, Engineering field-insensitive molecular clock transitions for symmetry violation searches (2023).
  - [10] G. Higgins, S. Salim, C. Zhang, H. Parke, F. Pokorny, and M. Hennrich, Micromotion minimization using ramsey interferometry, *New Journal of Physics* **23**, 123028 (2021).
  - [11] D. P. Nadlinger, P. Drmota, D. Main, B. C. Nichol, G. Araneda, R. Srinivas, L. J. Stephenson, C. J. Ballance, and D. M. Lucas, Micromotion minimisation by synchronous detection of parametrically excited motion (2021), 2107.00056 [physics, physics:quant-ph].
  - [12] L. Anderegg, B. L. Augenbraun, E. Chae, B. Hemmerling, N. R. Hutzler, A. Ravi, A. Collopy, J. Ye, W. Ketterle, and J. M. Doyle, Radio frequency magneto-optical trapping of CaF with high density, *Phys. Rev. Lett.* **119**, 103201 (2017).
  - [13] A. Omran, H. Levine, A. Keesling, G. Semeghini, T. T. Wang, S. Ebadi, H. Bernien, A. S. Zibrov, H. Pichler, S. Choi, J. Cui, M. Rossignolo, P. Rembold, S. Montangero, T. Calarco, M. Endres, M. Greiner, V. Vuletić, and M. D. Lukin, Generation and manipulation of schrödinger cat states in rydberg atom arrays, *Science* **365**, 570 (2019).
  - [14] H. J. Briegel and R. Raussendorf, Persistent entanglement in arrays of interacting particles, *Phys. Rev. Lett.* **86**, 910 (2001).
  - [15] R. Verresen, N. Tantivasadakarn, and A. Vishwanath, Efficiently preparing Schrödinger’s cat, fractons and non-abelian topological order in quantum devices (2022), 2112.03061 [cond-mat, physics:physics, physics:quant-ph].
  - [16] J. Y. Lee, W. Ji, Z. Bi, and M. P. A. Fisher, Decoding measurement-prepared quantum phases and transitions: from ising model to gauge theory, and beyond (2022), 2208.11699 [cond-mat, physics:quant-ph].
  - [17] T. V. Tscherbul, J. Ye, and A. M. Rey, Robust nuclear spin entanglement via dipolar interactions in polar molecules, *Phys. Rev. Lett.* **130**, 143002 (2023).
  - [18] D. Leibfried, E. Knill, S. Seidelin, J. Britton, R. B. Blakestad, J. Chiaverini, D. B. Hume, W. M. Itano, J. D. Jost, C. Langer, R. Ozeri, R. Reichle, and D. J. Wineland, Creation of a six-atom ‘schrödinger cat’ state, *Nature* **438**, 639 (2005).
  - [19] C. M. Holland, Y. Lu, and L. W. Cheuk, On-demand entanglement of molecules in a reconfigurable optical tweezer array (2022), arXiv:2210.06309.
  - [20] Y. Bao, S. S. Yu, L. Anderegg, E. Chae, W. Ketterle, K.-K. Ni, and J. M. Doyle, Dipolar spin-exchange and entanglement between molecules in an optical tweezer array (2022), arXiv:2211.09780.
  - [21] Y. Lin, D. R. Leibbrandt, D. Leibfried, and C.-w. Chou, Quantum entanglement between an atom and a molecule, *Nature* **581**, 273 (2020).
  - [22] Y. Zhou, Y. Shagam, W. B. Cairncross, K. B. Ng, T. S. Roussy, T. Grogan, K. Boyce, A. Vigil, M. Pettine, T. Zelevinsky, J. Ye, and E. A. Cornell, Second-scale coherence measured at the quantum projection noise limit with hundreds of molecular ions, *Phys. Rev. Lett.* **124**, 053201 (2020).
  - [23] P. D. Gregory, L. M. Fernley, A. L. Tao, S. L. Bromley, J. Stepp, Z. Zhang, S. Kotochigova, K. R. A. Hazzard, and S. L. Cornish, Second-scale rotational coherence and dipolar interactions in a gas of ultracold polar molecules, arXiv:2306.02991 (2023).
  - [24] C. Zhang, F. Pokorny, W. Li, G. Higgins, A. Pöschl, I. Lesanovsky, and M. Hennrich, Submicrosecond entangling gate between trapped ions via rydberg interaction, *Nature* **580**, 345 (2020).
  - [25] A. Sunaga, M. Abe, M. Hada, and B. P. Das, Merits of heavy-heavy diatomic molecules for electron electric-dipole-moment searches, *Physical Review A* **99**, 062506 (2019).
  - [26] T. Fleig and D. DeMille, Theoretical aspects of radium-containing molecules amenable to assembly from laser-cooled atoms for new physics searches, *New Journal of Physics* **23**, 113039 (2021).
  - [27] M. Śmiałkowski and M. Tomza, Highly polar molecules consisting of a copper or silver atom interacting with an alkali-metal

- or alkaline-earth-metal atom, *Physical Review A* **103**, 022802 (2021).
- [28] V. Andreev, D. G. Ang, D. DeMille, J. M. Doyle, G. Gabrielse, J. Haefner, N. R. Hutzler, Z. Lasner, C. Meisenhelder, B. R. O’Leary, C. D. Panda, A. D. West, E. P. West, and X. Wu, Improved limit on the electric dipole moment of the electron, *Nature* **562**, 355 (2018).
  - [29] T. S. Roussy, L. Caldwell, T. Wright, W. B. Cairncross, Y. Shagam, K. B. Ng, N. Schlossberger, S. Y. Park, A. Wang, J. Ye, and E. A. Cornell, An improved bound on the electron’s electric dipole moment (2023).
  - [30] B. L. Augenbraun, J. M. Doyle, T. Zelevinsky, and I. Kozryyev, Molecular asymmetry and optical cycling: laser cooling asymmetric top molecules, *Phys. Rev. X* **10**, 031022 (2020).
  - [31] B. L. Augenbraun, Z. D. Lasner, A. Frenett, H. Sawaoka, A. T. Le, J. M. Doyle, and T. C. Steimle, Observation and laser spectroscopy of ytterbium monomethoxide,  $\text{YbOCH}_3$ , *Phys. Rev. A* **103**, 022814 (2020).
  - [32] J. J. Hudson, B. E. Sauer, M. R. Tarbutt, and E. A. Hinds, Measurement of the electron electric dipole moment using ybf molecules, *Phys. Rev. Lett.* **89**, 023003 (2002).
  - [33] J. Lim, J. R. Almond, M. R. Tarbutt, D. T. Nguyen, and T. C. Steimle, The  $[557]\text{-X}^2\Sigma^+$  and  $[561]\text{-X}^2\Sigma^+$  bands of ytterbium fluoride,  $^{174}\text{YbF}$ , *J. Mol. Spectrosc.* **338**, 81 (2017).
  - [34] P. Aggarwal, H. L. Bethlem, A. Borschevsky, M. Denis, K. Esajas, P. A. B. Haase, Y. Hao, S. Hoekstra, K. Jungmann, T. B. Meijknecht, M. C. Mooij, R. G. E. Timmermans, W. Ubachs, L. Willmann, and A. Zapara, Measuring the electric dipole moment of the electron in BaF, *Eur. Phys. J. D* **72**, 197 (2018).
  - [35] T. C. Steimle, S. Frey, A. Le, D. DeMille, D. A. Rahmlo, and C. Linton, Molecular-beam optical Stark and Zeeman study of the  $\text{A}^2\Pi\text{-X}^2\Sigma^+(0,0)$  band system of BaF, *Physical Review A* **84**, 012508 (2011).
  - [36] T. A. Isaev, S. Hoekstra, and R. Berger, Laser-cooled raf as a promising candidate to measure molecular parity violation, *Phys. Rev. A* **82**, 052521 (2010).
  - [37] R. F. G. Ruiz, R. Berger, J. Billowes, C. L. Binnersley, M. L. Bissell, A. A. Breier, A. J. Brinson, K. Chrysalidis, T. E. Cocolios, B. S. Cooper, K. T. Flanagan, T. F. Giesen, R. P. de Groote, S. Franchoo, F. P. Gustafsson, T. A. Isaev, A. Koszorus, G. Neyens, H. A. Perrett, C. M. Ricketts, S. Rothe, L. Schweikhard, A. R. Vernon, K. D. A. Wendt, F. Wienholtz, S. G. Wilkins, and X. F. Yang, Spectroscopy of short-lived radioactive molecules, *Nature* **581**, 396 (2020).
  - [38] S.-M. Udrescu, S. Wilkins, A. Breier, R. F. G. Ruiz, M. Athanasakis-Kaklamanakis, M. Au, I. Belošević, R. Berger, M. Bissell, K. Chrysalidis, T. Cocolios, R. Groote, A. Dorne, K. Flanagan, S. Franchoo, K. Gaul, S. Geldhof, T. Giesen, D. Hanstorp, R. Heinke, A. Koszorus, S. Kujanpää, L. Lalanne, G. Neyens, M. Nichols, H. Perrett, J. Reilly, S. Rothe, B. V. D. Borne, Q. Wang, J. Wessolek, X. Yang, and C. Zülch, Precision spectroscopy and laser cooling scheme of a radium-containing molecule (2023).
  - [39] N. E. Shafer-Ray, Possibility of 0- $g$ -factor paramagnetic molecules for measurement of the electron’s electric dipole moment, *Physical Review A* **73**, 034102 (2006), publisher: American Physical Society.
  - [40] R. J. Mawhorter, B. S. Murphy, A. L. Baum, T. J. Sears, T. Yang, P. M. Rupasinghe, C. P. McRaven, N. E. Shafer-Ray, L. D. Alphe, and J.-U. Grabow, Characterization of the ground  $\text{X}_1$  state of  $^{204}\text{Pb}^{19}\text{F}$ ,  $^{206}\text{Pb}^{19}\text{F}$ ,  $^{207}\text{Pb}^{19}\text{F}$ , and  $^{208}\text{Pb}^{19}\text{F}$ , *Physical Review A* **84**, 022508 (2011).
  - [41] C. Zhu, H. Wang, B. Chen, Y. Chen, T. Yang, J. Yin, and J. Liu, Fine and hyperfine interactions of PbF studied by laser-induced fluorescence spectroscopy, *The Journal of Chemical Physics* **157**, 084307 (2022).